Theoretical study of phosphorous δ-doped silicon for quantum computing

Gefei Qian,[1] Yia-Chung Chang,[1] and J. R. Tucker[2]

[1]*Department of Physics, University of Illinois at Urbana-Champaign, 1110 West Green Street, Urbana, Illinois 61801, USA*
[2]*Department of Electrical Engineering, University of Illinois at Urbana-Champaign, Urbana, Illinois 61801, USA*
(Received 20 July 2004; revised manuscript received 28 October 2004; published 12 January 2005)

We present microscopic model calculations of phosphorous δ-doped silicon. Using the planar Wannier orbitals [Y. C. Chang and G. Li, Comput. Phys. Commun. **95**, 158 (1996)] obtained based on the pseudopotential method, we calculate the electronic structures of a large slab (1000 ML) self-consistently (for doping electrons), taking into account both the long-range Coulomb potential in the direction perpendicular to the doping plane and the short-range interaction due to the 1/4 monolayer (ML) phosphor δ doping. Our results show that the Fermi level after doping is about 100 meV below silicon conduction band minimum (CBM). We also find that the short-range interaction due to P dopants only has a minor influence on the Fermi level.

I. INTRODUCTION

Quantum computation[1–4] has attracted tremendous interest in recent years. There have been numerous proposals for the implementation of a scalable quantum computer. One of them is the silicon-based architecture proposed by Kane,[5] which uses the phosphorus nuclear spin as the quantum bit (qubit). In this architecture, a phosphorus donor in Si is placed $\sim$200 Å beneath a narrow conducting gate (A gate). A single nonbonding (conduction band) electron occupies the hydrogen-like ground state with an average Bohr radius of $\sim$25 Å. Voltage applied to an A gate displaces this electron cloud away from its P-atom nucleus, decreasing the hyperfine interaction and lowering the nuclear magnetic resonance (NMR) frequency in a dc magnetic field of $\sim$2 T. Individual P nuclei can thereby be brought into resonance with an in-plane ac magnetic field, permitting arbitrary spin rotations to be performed on any single qubit using an appropriate sequence of gate pulses. Additional J gates, located between the P-atom donors of a planar array, would be used to induce exchange coupling for two-qubit operations via overlap of their electron wave functions. Results of quantum computation would eventually be read out by detecting the presence or absence of electronic polarizations induced onto target donors by differential gate biasing when coupled to an output qubit, thereby determining overall wavefunction parity for a two-electron ground state as adiabatically dictated by the donor nuclear spins for strong J gate coupling.

More recently Vrijen *et al.* suggest using only the electron spins of the isolated donors for quantum computation.[4] By taking advantage of g-factor variations available in SiGe heterolayers (Si: $g = 1.998$, Ge: $g = 1.563$), electron spins could be selectively tuned in and out of resonance under gate control. Bias voltages applied to an individual gate displace the bound electron with respect to its P-atom nucleus, just as in the proposal by Kane; but in this case the electron's wave function can sample layers of different alloy composition and g factor, bringing its spin in and out of resonance for single-qubit ESR rotations. Larger gate biases would be employed to couple neighboring qubits by displacing their bound electrons even farther into Ge-rich layers, lowering their binding energies and substantially increasing the spatial extent of

their wave functions. Separate J gates between each pair of donors could thereby be eliminated, along with the delicate adiabatic transfers of spin information from nuclei to electrons which are required under Kane's original proposal. Utilization of the electron spins in place of donor nuclear spins has several other potential advantages: (1) higher ESR frequencies could permit much faster single-qubit operations up to 1 GHz, (2) the electron spins can be fully polarized at realizable magnetic fields and temperatures, establishing a well-characterized starting point for quantum calculations, and (3) isotopic purity is no longer an absolute requirement.

The realization of the abovementioned Si-based quantum computers depends on three critical issues. (1) Individual P-atom donors must be accurately positioned into planar arrays with a tolerance of 10 Å (smaller than the 25 Å Bohr radius). (2) Each donor within the array must be epitaxially encapsulated into Si or SiGe with no nearby charged defects, surface states, or dangling bonds which might otherwise offset the bound electron charge distributions. (3) A single-electron transistor (or comparably small FET channel) must be incorporated very close to each read-out qubit, in order to sense the extremely small charge displacements for electrically polarized spin singlets under differential gate biasing.

One possible process for selectively patterning individual donors, and larger self-ordered arrays, with atomic precision is to use atom-resolved scanning-tunneling microscopy (STM) lithography on hydrogen-terminated silicon.[6–8] Atomically clean surfaces are prepared in ultrahigh vacuum (UHV) and passivated *in situ*, with one hydrogen atom attached to each silicon dangling bond to form a single-monolayer "H-atom resist." In tunneling mode, the STM's electron beam is confined to atomic dimensions, and hydrogen atoms can be removed by scanning at voltage and current levels higher than those used for imaging.

Phosphorous donor atoms can be selectively deposited onto the STM-exposed areas by adsorption of individual PH_3 precursor molecules.[8] Phosphine does not adsorb on H-terminated surfaces at room temperature, and substrates must be heated above 500 °C to evolve hydrogen and expose bare Si dangling bonds in order to sustain common chemical vapor deposition reactions involving SiH_4, PH_3, B_2H_6, and related molecular species. On the other hand, recent STM

imaging and surface studies have shown that PH$_3$ is readily adsorbed onto bare Si(100)-2×1 dimers at alternating sites along a single row.[9,10] Over extended areas of the bare surface, the PH$_3$ adsorption sites are staggered between adjacent rows to form a self-ordered ~1/4 ML $c(2\times2)$ adlayer (with ~50 Å domains) at saturation coverage. By using the STM to expose bare Si dangling bonds on a H-terminated surface, selected areas can be targeted for self-ordered PH$_3$ deposition. Overgrowth of the self-ordered PH$_3$ precursor layers will yield a new type of ultradense 2D electron gas. Because we need to selectively pattern such layers into atom-scale devices, a detailed understanding of their electronic structure is essential.

Previously, several theoretical studies of n-type δ-doping layers in Si based on the effective mass approximation have been reported.[11–13] The main deficiency in the effective mass approximation is that it fails to describe properly the intervalley couplings introduced by the self-consistent confining potential. Furthermore, at doping density as high as 1/4 ML as considered here, it is not clear how serious an effect the short-range part of the doping potential will have. In this paper, we perform microscopic model calculations of phosphorous δ-doped silicon within an empirical pseudopotential method. We consider a 1/4 monolayer (ML) phosphorous δ-doping sheet with (2×2) configuration embedded in a large slab (1000 ML) of Si. The electronic structures of δ-doped Si are calculated within a planar Wannier-orbital (PWO) basis, which is constructed via linear combinations of the products of two-dimensional plane waves and one-dimensional Gaussian functions.[14] This basis is particularly suited for planar structures including surfaces, interfaces, superlattices, and δ-doped systems as considered here. Due to the localized nature (along the perpendicular axis) of the PWO's, the Hamiltonian matrix is sparse; thus, it can be solved efficiently. Our results show that the Fermi level after doping is about 100 meV below silicon conduction band minimum (CBM). We also examined the effects of the short-range interaction due to P dopants and find that it only has a minor influence on the band structures of the system. This implies that at current doping density, the charge distribution is not very sensitive to the in-plane doping pattern. Our results are important for understanding the electronic structures of nanoscale devices such as Si-based quantum computer.

II. METHOD OF CALCULATION

A. Hamiltonian for doping electrons

The electronic states of the δ-doped Si are expanded in terms of planar Wannier-orbitals (PWO's) as described in Ref. 14. A PWO is defined as[14]

$$\langle \rho, z | W_{n\mathbf{k}_s}(l_z) \rangle = \sqrt{\frac{1}{N_{2D}\sigma_{cell}}} \sum_{\substack{\nu,\alpha,\sigma \\ \mathbf{G}_\parallel}} e^{-i(\mathbf{G}_\parallel + \mathbf{G}_s + \mathbf{k}_\parallel)\cdot\rho}$$

$$\times C^w_{n\mathbf{k}_s}(\alpha,\nu,\sigma) f^{\sigma,l_z}_{\alpha,\nu}(z) I_p(\mathbf{G}_\parallel, l_z), \quad (1)$$

where, C^w's are Wannier-orbital coefficients as obtained in Ref. 14, N_{2D} denotes the number of unit cells in the in-plane
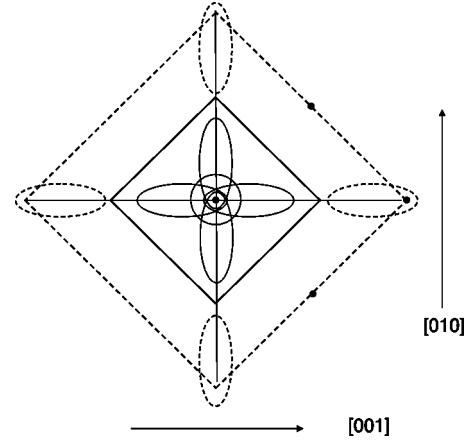

FIG. 1. Schematic diagram of the 1×1 (dashed) and $c(2\times2)$ Brillouin zones (solid) for Si (001) surface. The constant energy surfaces for the six equivalent valleys projected in the 1×1 surface BZ are shown as dashed ellipses (for the x, y valleys) and a circle at the center (for the two z valleys).

direction of the system, while σ_{cell} is the area of the planar (2D) unit cell. Note that a Löwdin orthogonalization procedure (see Appendix of Ref. 14) has been used to convert the nonorthogonal PWO basis into the orthogonal PWO basis. In the above formula, $\mathbf{G}_\parallel$ is a 2D reciprocal lattice vector of the corresponding bulk (1×1) system, $\mathbf{G}_s$ is a 2D reciprocal lattice vector for the 2D δ-doped (2×2) system enclosed within the bulk 2D Brillouin zone (BZ) (indicated as dark circles in Fig. 1), and $\mathbf{k}_\parallel$ is a sampling $\mathbf{k}$ vector in the 2D BZ of the (2×2) system. Therefore, we have $\mathbf{k}_s \equiv \mathbf{G}_s + \mathbf{k}_\parallel$. The phase factor $I_p(\mathbf{G}_\parallel, l_z)$, which for an fcc lattice, is determined by [see Eq. 17 in Ref 14],

$$I_p = \begin{cases} -1 & \text{if } G_x/(2\pi/a) \text{ and } l_z \text{ are both odd,} \\ 1 & \text{otherwise.} \end{cases} \quad (2)$$

$$f^{\sigma,l_z}_{\alpha,\nu}(z) = \left[\sqrt{\frac{\pi}{2\alpha}}\left(\frac{1}{4\alpha}\right)^\nu \right]^{-1/2} [z - z_\sigma - z(l_z)]^\nu e^{-\alpha[z - z_\sigma - z(l_z)]^2}, \quad (3)$$

where $\nu = 0,1$ for even and odd basis functions. The exponents (α) are chosen to be

$$\{\alpha^s_1, \alpha^s_2, \alpha^p_1, \alpha^p_2\} = \{0.3, 0.75, 0.5, 1.5\},$$

in units of Bohr^{-2}. There are two schemes to construct the Gaussian functions. One is at the atomic site (on-site), the other at the bond center (on bond). For the on-site scheme, $z_\sigma = (\sigma-1)a/4$; $\sigma = 1,2$. For the on-bond scheme, $z_\sigma = (\sigma-1)a/4 - a/8$; $\sigma = 1,2$. In this study, the on-bond scheme is used. In the above equations, l_z is the label of each atomic layer, while $z(l_z)$ is the coordinate of the l_z layer with the origin set at the doping layer.

The Hamiltonian for doping electrons in the δ-doped Si can be written as a sum of the bulk Hamiltonian (H_0) and the doping potential (V_{dop}) plus the electron-electron interaction (v_{ee}) screened by the valence electrons. We write

$$V_{\text{dop}}(\mathbf{r}) = \sum_{\mathbf{R}_\parallel} V_d(\mathbf{r} - \mathbf{R}_\parallel), \tag{4}$$

where $V_d(\mathbf{r})$ is the difference in atomic pseudopotentials between P dopant and Si host atoms at each doping site, screened by the valence electrons. In the Fourier space, the doping potential takes the form

$$\widetilde{V}_{\text{dop}}(\mathbf{q}) = \sum_{R_\parallel} e^{-i\mathbf{q}\cdot\mathbf{R}_\parallel}\widetilde{V}_d(\mathbf{q}), \tag{5}$$

where

$$\widetilde{V}_d(\mathbf{q}) = -\frac{8\pi}{\varepsilon(\mathbf{q})\mathbf{q}^2} + \widetilde{V}_{\text{ps}}(\mathbf{q}).$$

Throughout this paper, we have scaled all energy quantities in units of Rydbergs and distance in Bohrs such that $\hbar^2/2m_0 = 1$, where m_0 is the free electron mass. $\varepsilon(q)$ is the static dielectric function due to the valence electrons, which can be approximated by the following analytic form:[15]

$$\frac{1}{\varepsilon(\mathbf{q})} = \frac{1}{\varepsilon(0)} + A\frac{\mathbf{q}^2}{(\mathbf{q}^2 + \gamma_1^2)} + (1-A)\frac{\mathbf{q}^2}{(\mathbf{q}^2 + \gamma_2^2)}$$
$$- \frac{1}{\varepsilon(0)}\frac{\mathbf{q}^2}{(\mathbf{q}^2 + \gamma_3^2)}, \tag{6}$$

where $\varepsilon(0) = 11.4$, $A = 1.133$, $\gamma_1 = 0.798$, $\gamma_2 = 0.440$, and $\gamma_3 = 2.645$ in atomic units. $\widetilde{V}_{\text{ps}}(\mathbf{q})$ denotes the pseudopotential modification to the $1/r$ potential. For phosphorous donor in Si, it has been shown that $V_d(\mathbf{r})$ is well approximated by a point-charge model,[16] i.e., V_{ps} is negligible. Similarly, the screened electron-electron interaction is given by

$$\widetilde{v}_{ee}(\mathbf{q}) = \frac{8\pi}{\varepsilon(\mathbf{q})\mathbf{q}^2}.$$

Adopting the Kohn-Sham density-functional theory[17] for the doping electrons, we obtain the following effective Schrödinger equation:

$$\{H_0 + V_{\text{dop}}(\mathbf{r}) + V_H(\mathbf{r}) + V_{\text{xc}}[\rho(\mathbf{r})]\}\psi(\mathbf{r}) = E\psi(\mathbf{r}), \tag{7}$$

where V_H is the self-consistent Hartree potential associated with v_{ee} and $V_{\text{xc}}[n(\mathbf{r})]$ is the exchange-correlation potential within local density approximation (LDA). The above equation is solved by expanding $\psi(\mathbf{r})$ in terms of orthogonalized PWO's, which translates the differential equation into a finite-dimension eigenvalue problem. Because the coupling between PWO's separated by a distance larger than the fifth neighbor is negligibly small, the above Hamiltonian matrix becomes a band matrix, which can be diagonalized quite efficiently with the standard LAPACK library routines. Thus, we can handle a large-size (~1000 ML) slab 16 PWO's in each monolayer.

The matrix elements between any two PWO's for H_0 are given by

$$\langle W_{n\mathbf{k}_s}(l_z)|H_0|W_{n'\mathbf{k}_{s'}}(l_z')\rangle = \sum_{\mathbf{G}_\parallel,\mathbf{G}_\parallel'}\int\frac{d\rho}{N_{\text{2D}}\sigma_{cell}}e^{-i(\mathbf{G}_\parallel-\mathbf{G}_\parallel'+\mathbf{G}_s-\mathbf{G}_s')\rho}$$
$$\times\sum_{\substack{\alpha\nu\sigma\\\alpha'\nu'\sigma'}}\int dz f^{\sigma'l_z'}_{\alpha'\nu'}(z)H_0 f^{\sigma l_z}_{\alpha\nu}(z)$$
$$\times C^w_{n\mathbf{k}_s}(\alpha,\nu,\sigma)C^w_{n'\mathbf{k}_{s'}}(\alpha',\nu',\sigma')$$
$$\equiv H_0(n,l_z,n',l_z')\delta_{ss'}. \tag{8}$$

Because the bulk Hamiltonian H_0 is invariant under translation of a lattice vector, we have

$$H_0(n,n',l_z'-l_z) \equiv H_0(n,l_z+l,n',l_z'+l) \tag{9}$$

with l being an arbitrary atomic layer. Details of $H_0(n,n',l_z)$ have been described in Ref. 14.

The matrix elements between any two PWO's for $V_{\text{dop}}(\mathbf{r})$ are given by

$$\langle W_{n\mathbf{k}_s}(l_z)|V_{\text{dop}}(\mathbf{r})|W_{n'\mathbf{k}_{s'}}(l_z')\rangle = \int\frac{d^3q}{(2\pi)^3}V_{\text{dop}}(\mathbf{q})$$
$$\times\langle W_{n\mathbf{k}_s}(l_z)|e^{i\mathbf{q}\cdot\mathbf{r}}|W_{n'\mathbf{k}_{s'}}(l_z')\rangle$$
$$= C_0|l_z|\delta_{nn'}\delta_{l_z,l_z'}\delta_{ss'} - U_0(\mathbf{k}_\parallel,n,n',l_z,l_z',\mathbf{G}_s,\mathbf{G}_{s'}) - C(\infty), \tag{10}$$

where $C_0 = 2a\pi Q/\varepsilon(0)\sigma_{\text{cell}}$, where Q is the average doping charge in a 2D unit cell. The first term on the right-hand side describes the contribution of the long-range Coulomb interaction originated from the δ-doping sheet, which is represented by a constant average charge density. The second term, U_0 captures the short-range contribution and the difference caused by replacing the discrete dopant charges by a constant average charge density, which is also short range in nature. Note that the presence of U_0 leads to coupling between states associated with different $\mathbf{G}_s$. For a (2×2) configuration considered here, there are four different $\mathbf{G}_s$. The last term, $C(\infty)$ corresponds to the self-interaction Coulomb energy of an infinite charged sheet, which will be cancelled exactly by a corresponding term from the Hartree potential. Detailed derivation for the above expression is given in the Appendix.

To reduce computation effort, we solve the problem in a two-step method. In the first step, we ignore the presence of U_0, which allows us to decouple states associated with different $\mathbf{G}_s$. Thus, the size of the Hamiltonian matrix is reduced by a factor four. Furthermore, we replace the 3D charge density $\rho(\mathbf{r})$ by an in-plane averaged charge density $\rho_0(z)$. In this way, the results obtained in step 1 can be directly compared with those obtained from a multivalleyed effective-mass model. In the second step, we use the eigenstates obtained in the first step (with energies within a selected range) as a new reduced basis. We then solve the full problem within the reduced basis.

The matrix elements for exchange-correlation energy V_{xc} is approximated by

$$\langle W_{n',l_z',\mathbf{G}_{s'}+\mathbf{k}_\parallel}|V_{\text{xc}}[\rho(z)]|W_{n,l_z,\mathbf{G}_s+\mathbf{k}_\parallel}\rangle$$

$$= V_{\text{xc}}(l_z)\langle W_{n',l_z',\mathbf{G}_{s'}+\mathbf{k}_\parallel}|W_{n,l_z,\mathbf{G}_s+\mathbf{k}_\parallel}\rangle$$

$$= V_{\text{xc}}(l_z)\,\delta_{ss'}\,\delta_{n'n}\,\delta_{l_z',l_z}, \tag{11}$$

since $V_{\text{xc}}[\rho(z)]$ is a slow varying function of z, which can be approximated by its value at l_z.

The exchange-correlation energy, in the reduced basis, is expressed as

$$V_{\text{xc}}(j,i) = \sum_{l_z} V_{\text{xc}}(l_z)\sum_{n,\mathbf{G}_s}[C^0_{j,\mathbf{G}_s}(n,l_z)]^* C^0_{i,\mathbf{G}_s}(n,l_z), \tag{12}$$

where $C^0_{i,\mathbf{G}_s}(n,l_z)$ is the expansion coefficient of the eigenstates obtained in step 1 in terms of PWO's. The exchange-correlation energy is evaluated within DFT-LDA. We use the XC functional calculated by Ceperley and Alder[18] and parametrized by Zunger and Perdew.[19] The energy and charge density are rescaled according to

$$E = \frac{\bar{m}}{\varepsilon_0}\tilde{E}, \quad \rho(z) = \left(\frac{\bar{m}}{\varepsilon_0}\right)^3 \tilde{\rho}(z),$$

so that the XC functional derived for electrons with spherical mass can apply. Here $\bar{m} = \sqrt[3]{(m_t^*)^2 m_l^*}$ denotes the spherical average of the density-of-states effective mass,[20] and $\varepsilon_0 = \varepsilon(0)$ is the long-wavelength dielectric constant. The effect of intervalley scattering among six different pockets has been ignored.[21] Therefore, the charge density enters the XC functional is the charge density per pocket. This approximation is reasonable, because the exchange interaction is proportional to $1/\Delta k^2$, where Δk is the difference in momentum between two pockets, which is quite large.

B. The Hartree term

The self-consistent Hartree potential seen by a doping electron is given by[22]

$$V_H(\mathbf{r}) = \int \frac{d^3\mathbf{q}}{(2\pi)^3}\frac{8\pi\rho_e(\mathbf{q})}{q^2\varepsilon(\mathbf{q})}e^{i\mathbf{q}\cdot\mathbf{r}}, \tag{13}$$

where

$$\rho_e(\mathbf{q}) = \int d^3\mathbf{r}\cdot e^{-i\mathbf{q}\cdot\mathbf{r}}\rho_e(\mathbf{r})$$

is the Fourier transform of the electron charge density (for doping electrons only).

Due to the in-plane translational invariance of the electron charge density, $\rho_e(\mathbf{q})$ is nonvanishing only at $\mathbf{q}_\parallel = \mathbf{G}_\parallel$, where $\mathbf{G}_\parallel$ is some reciprocal lattice vector of the 2D lattice. Thus, Eq. (13) becomes

$$V_H(\mathbf{r}) = \frac{1}{\sigma_{\text{cell}}}\int\frac{dq_z}{(2\pi)}\sum_{\mathbf{G}_\parallel}\frac{8\pi\rho_e(\mathbf{G}_\parallel + q_z\hat{z})}{(\mathbf{G}_\parallel^2 + q_z^2)\varepsilon(\sqrt{\mathbf{G}_\parallel^2 + q_z^2})}e^{iq_z z}, \tag{14}$$

where σ_{cell} is the surface unit cell area as defined before. Since the long-range Coulomb potential is dominated by small q, we can ignore the contribution from the $\mathbf{G}_\parallel \neq 0$

("Umklapp") terms. With this approximation, we have

$$V_H(z) = \frac{4\pi}{\varepsilon(0)}\int dz'\rho_e(z')|z-z'|, \tag{15}$$

where $\rho_e(z)$ is the in-plane averaged electron charge density

$$\rho_e(z) \equiv \frac{1}{\sigma_{\text{cell}}\Delta_z}\rho_e(l_z). \tag{16}$$

Δ_z is the layer thickness in the z direction and $\rho_e(l_z)$ is the in-plane averaged electron occupation at atomic layer l_z, which is given by

$$\rho_e(l_z) = \sum_{m,\mathbf{k}_\parallel} w_{\mathbf{k}_\parallel}\rho_m^{\mathbf{k}_\parallel}(l_z)\theta[E_F - E_m(\mathbf{k}_\parallel)], \tag{17}$$

where $w_{\mathbf{k}_\parallel}$ is the weighting factor and

$$\rho_m^{\mathbf{k}_\parallel}(l_z) = \sum_{n,s}|C^m_{n,\mathbf{G}_s+\mathbf{k}_\parallel}(l_z)|^2, \tag{18}$$

where Δ_z is the layer thickness in the z direction and $C^m_{n,\mathbf{G}_s+\mathbf{k}_\parallel}(l_z)$ is the expansion coefficient of the mth eigenstate of the δ-doped Si in terms of PWO's.

The matrix elements between any two PWO's for $V_H(z)$ are given by

$$\langle W_{n\mathbf{k}_s}(l_z)|V_H(z)|W_{n'\mathbf{k}_s}(l_z')\rangle = V_H(l_z)\delta_{nn'}\delta_{l_z,l_z'}\delta_{ss'} + C(\infty), \tag{19}$$

where we have used the property that $V_H(z)$ is a slow varying function over an atomic distance and the fact that the PWO's are orthogonal. The last term $C(\infty)$ describes the self-interaction, which cancels the corresponding term for V_{dop} exactly.

C. Fermi filling

Within parabolic approximation, the energy dispersion (in Ry) for each 2D subband in the vicinity of Γ and Δ points, respectively, is given by

$$E_i(\mathbf{k}) = E_i^{(\Gamma)} + \frac{\mathbf{k}^2}{m_t^*},$$

$$E_i(\mathbf{k}) = E_i^{(\Delta)} + \frac{(\mathbf{k}_x - \mathbf{k}^\Delta)^2}{m_l^*} + \frac{(\mathbf{k}_y)^2}{m_t^*}, \tag{20}$$

where m_t^* and m_l^* are the transverse and longitudinal effective masses, respectively, which are obtained by fitting the curvature of each subband calculated by the present method. For bulk Si, we obtain $m_t^* = 0.192$ and $m_l^* = 0.916$, in good agreement with experimental values. For subbands in δ-doped Si, these values are slightly modified. We obtain $m_t^* = 0.211$ and $m_l^* = 0.95$. Here the spin-orbit splitting has been ignored, i.e., each subband has a twofold spin degeneracy. For 2D electron gas, the 2D electron density is given by

$$\sigma_d = n_e = 2\int\frac{d^2\mathbf{k}}{(2\pi)^2}\sum_i^n\theta[E_F - E_i(\mathbf{k})], \tag{21}$$

where E_F is the Fermi level:

$$\sigma_d = \frac{m_t^*}{2\pi}\left[\sum_i^{n^\Gamma}(E_f - E_i^\Gamma) + 4\sqrt{\frac{m_l^*}{m_t^*}}\sum_i^{n^\Delta}(E_f - E_i^\Delta)\right]. \quad (22)$$

The factor 4 appearing in the last term is due to the fact that there are four equivalent Δ pockets in the x-y plane.

By rearranging the formulas above, we have

$$2\pi\sigma_d = (m_t^* n^\Gamma + 4\sqrt{m_l^* m_t^*}\, n^\Delta)E_f$$
$$- \left(m_t^*\sum_i^{n^\Gamma}E_i^\Gamma + 4\sqrt{m_l^* m_t^*}\sum_i^{n^\Delta}E_i^\Delta\right), \quad (23)$$

from which we get the expression for the Fermi energy

$$E_f = \frac{2\pi\sigma_d + m_t^*\sum_i^{n^\Gamma}E_i^\Gamma + 4\sqrt{m_l^* m_t^*}\sum_i^{n^\Delta}E_i^\Delta}{m_t^* n^\Gamma + 4\sqrt{m_l^* * m_t^*}\, n^\Delta}. \quad (24)$$

In the above derivation, we have used the fact that

$$(\Delta\mathbf{k}_i^\Gamma)^2 = m_t^*(E_f - E_i^\Gamma),$$
$$(\Delta\mathbf{k}_i^{\Delta x})^2 = m_l^*(E_f - E_i^\Delta), \quad (25)$$
$$(\Delta\mathbf{k}_i^{\Delta y})^2 = m_t^*(E_f - E_i^\Delta).$$

In the vicinity of Γ and Δ points, the parabolic approximation works very well, even when the filling goes beyond the Brillouin zone boundary in the vicinity of the Δ point. This means that the energy difference is mostly due to the kinetic energy, and the spatial distribution of wave functions does not change appreciably with $\mathbf{k}$. In this case the integration can be approximated by the area times the charge density for each occupied level at the pocket centers.

If we define $\rho(l_z)$ as the charge density distribution at atomic layer l_z, and $\rho_i^{(\Gamma,\Delta)}(l_z)$ the probability distribution in each state, we have

$$\rho(l_z) = \frac{1}{\pi a}\left[\sum_i^{n^\Gamma}(\mathbf{k}_i^\Gamma)^2\rho_i^\Gamma(l_z) + 4\sqrt{\frac{m_l^*}{m_t^*}}\sum_i^{n^\Delta}(\mathbf{k}_i^\Delta)^2\rho_i^\Delta(l_z)\right], \quad (26)$$

where $\mathbf{k}_i^2 \equiv (E_f - E_i)$. In practice, the Fermi level can be determined in a simpler way. Define

$$\sigma_d = f^\Gamma\sum_i^{n^\Gamma}(E_f - E_i^\Gamma) + f^\Delta\sum_i^{n^\Delta}(E_f - E_i^\Delta) \quad (27)$$

with filling factor for each state in the two pockets as

$$f^\Gamma = \frac{m_t^*}{2\pi}, \quad f^\Delta = \frac{4\sqrt{m_l^* m_t^*}}{2\pi}. \quad (28)$$

States derived from two z pockets are mixed by the doping potential and form two closely spaced levels at the Γ point in the 2D BZ, each with twofold degeneracy due to the spin. States derived from the four (x, y) pockets appear as levels at the Δ point in the 2D BZ. The four equivalent Δ valleys remain degenerate in addition to the twofold spin degeneracy. Thus, we have
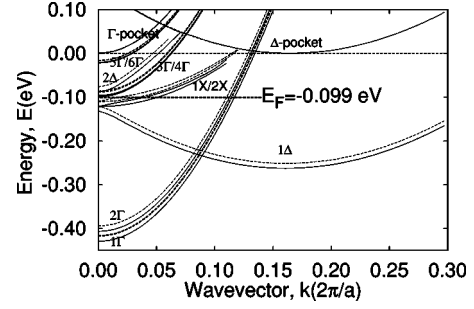

FIG. 2. Subband structures (for $k_x = 0 \sim 0.32\pi/a$) of the δ-doped Si with doping density of $1/4$ ML. The energy zero is placed at the conduction-band minimum of bulk Si. The solid lines show the band structure without the exchange-correlation and short-range effects, while the dotted lines show the band structure obtained in the full model.

$$E_f = \frac{1}{n^\Gamma f^\Gamma + n^\Delta f^\Delta}\left[\sigma_d + f^\Gamma\sum_i^{n^\Gamma}E_i^\Gamma + f^\Delta\sum_i^{n^\Delta}E_i^\Delta\right] \quad (29)$$

and

$$\rho(l_z) = \frac{2}{a}\left[f^\Gamma\sum_i^{n^\Gamma}(E_f - E_i^\Gamma)\rho_i^\Gamma(l_z) + f^\Delta\sum_i^{n^\Delta}(E_f - E_i^\Delta)\rho_i^\Delta(l_z)\right]. \quad (30)$$

At finite temperatures, the chemical potential μ is determined by

$$\sigma_d = \frac{2\pi}{4\pi^2}\left[\sum_i^{n^\Delta}\int\frac{d\mathbf{k}^2}{1 + e^{(E_i^\Delta - \mathbf{k}^2/m_t^* - \mu)/k_B T}}\right.$$
$$\left.+ \sqrt{\frac{m_l^*}{m_t^*}}\sum_i^{n^\Gamma}\int\frac{d\mathbf{k}^2}{1 + e^{(E_i^\Gamma - \mathbf{k}^2/m_t^* - \mu)/k_B T}}\right]. \quad (31)$$

Carrying out the integration yields

$$\sigma_d = \frac{k_B T}{2\pi}\left[m_t^*\sum_i^{n^\Gamma}\ln\frac{\alpha_i^\Gamma}{\alpha_i^\Gamma + 1} + \sqrt{m_t^* * m_l^*}\sum_i^{n^\Delta}\ln\frac{\alpha_i^\Delta}{\alpha_i^\Delta + 1}\right],$$

where $\alpha_i^\Gamma \equiv e^{(E_i^\Gamma - \mu)/k_B T}$ and $\alpha_i^\Delta \equiv e^{(E_i^\Delta - \mu)/k_B T}$. Once the chemical potential μ is determined, the filled charge distribution is given by

$$\rho(l_z) = \frac{k_B T}{a/2}\left[f^\Gamma\sum_i^{n^\Gamma}\ln\frac{\alpha_i^\Gamma}{\alpha_i^\Gamma + 1}\rho_i^\Gamma(l_z) + f^\Delta\sum_i^{n^\Delta}\ln\frac{\alpha_i^\Delta}{\alpha_i^\Delta + 1}\rho_i^\Delta(l_z)\right]. \quad (32)$$

III. RESULTS

The subband structure of the $1/4$ ML δ-doped Si obtained in step 1 (with long wavelength approximation) of the present model is shown as solid curves in Fig. 2. Only the region from the zone center to $k = 0.32\pi/a$ along the x direction is plotted. There is no extra structure from this point to

the zone boundary. The label $n\Gamma$ denotes the nth confined subband with subband minimum located at the Γ point (zone center), while $n\Delta$ denotes the nth confined subband with subband minimum located at the Δ point which is at $\mathbf{k}_\Delta = (0.165,0)(2\pi/a)$ in folded Brillouin zone. In bulk Si, the conduction band has six equivalent valleys with minima at $(\pm\mathbf{k}_\Delta,0,0)(2\pi/a)$, $(0,\pm\mathbf{k}_\Delta,0)(2\pi/a)$, and $(0,0,\pm\mathbf{k}_\Delta) \times (2\pi/a)$, where $\mathbf{k}_\Delta \sim 0.85$. With the present pseudopotential model, we obtain $\mathbf{k}_\Delta \sim 0.835$. The constant energy surfaces of the six equivalent valleys projected in the bulk 2D Brillouin zone are shown in Fig. 1. The four dashed ellipses denote the four valleys in the x-y plane, while the circle at the center denotes the two z valleys (projected into the surface BZ). Due to zone folding in the surface BZ for the (2 $\times 2$) system, the x and y Δ minima are folded to $[\pm(1 -\mathbf{k}_\Delta),0](2\pi/a)$, $[0,\pm(1-\mathbf{k}_\Delta)](2\pi/a)$. The constant energy surfaces of the four x,y valleys folded into the (2×2) 2D BZ are shown as solid ellipses in Fig. 1. The intervalley coupling caused by the doping potential gives rise to a mixing of the two folded z valleys (near the Γ point), which form two closely spaced subbands labeled as 1Γ and 2Γ in Fig. 2. The splitting between the two levels is about 20 meV.

The second conduction band of bulk Si becomes degenerate with the first conduction band at the X point. All six of these X-point states are folded to the zone center of the (2 $\times 2$) 2D BZ and they are mixed due to the doping potential. These six levels near the zone center are labeled 1Δ, 2Δ, $1X/2X$, and $3\Gamma/4\Gamma$, respectively, and they have different dispersion as seen in the figure. For the range of $\mathbf{k}$ considered in the figure, the 1Δ and 2Δ are derived from the two lowest conduction bands near the X point (along the x direction), the $1X/2X$ levels from the other X point (along the y direction), and the $3\Gamma/4\Gamma$ levels are from the third X point (along the z direction). The Fermi level (labeled E_F) obtained from the full calculations is also shown in the figure for the purpose of analyzing the carrier population. As seen in the figure, only the 1Γ, 2Γ, and four equivalent 1Δ valleys (only one out of four is shown here) have significant population (the $1X/2X$ subbands have a population less than 1% of the total), which justifies the analysis used in the previous section. Also note that the 1Δ subband becomes slightly nonparabolic for $\mathbf{k}$ near the zone center, which will cause a minor error in the determination of the Fermi level (on the order of a few meV).

To examine the effects of the short-range interaction, we also show in Fig. 2 the subband structures obtained by the full model (dashed lines). We see that the magnitudes of corrections due to U_{SR} are on the order of 10 meV and they are $\mathbf{k}_\parallel$ dependent, which leads to a slight correction (by about 1%) to the effective mass of each subband. Furthermore, the coupling of different $\mathbf{G}_s$ terms due to the short-range part (U_{SR}) of the doping potential leads to a mixing of the x-y valleys with the z valley, which appears as a weak anticrossing effect in the subband structure. This mixing, however, is far away from the subband minima; thus, it does not modify the parabolic shape of the valley significantly. We noticed that in the vicinity of the subband minima, the band structure is still well approximated by a parabola, which validates the effective-mass approximations used in determining the Fermi filling as discussed in the previous section.

TABLE I. Effect of the exchange-correlation (XC) and short range (SR) interaction on the Fermi level (E_F) (in meV), measured with respect to the conduction band minimum.

	Step 1	Step 1+XC	Step 1+XC+SR
E_F (meV)	−52	−111	−99

Table I shows the effect of exchange-correlation energy and the short-range interaction on the Fermi level (E_F) for the case without coupling of different $\mathbf{G}_s$ terms. The exchange-correlation effect lowers the Fermi level by ~ 60 meV, while the inclusion of the SR interaction increases the Fermi level by ~ 10 meV. After including both the XC and SR effects, the Fermi level is located at ~ 100 meV below the conduction band minimum (CBM) of bulk silicon.

Figure 3 shows the self-consistent potential of the 1/4 ML δ-doped Si calculated in step 1 (dashed curve) and with the full model (solid curve). The horizontal axis shows the z coordinate (in the direction perpendicular to the doping plane) in the units of Å. The potential displays a "V" shape, which is typical for δ-doped systems.[23] The horizontal lines indicate the confined energy levels below the Fermi level associated with the Γ subband and Δ subband. The number in the parentheses for the Δ subband indicates the valley degeneracy, since there are four equivalent valleys in the x-y plane. As seen in the figure, the inclusion of both XC and SR effects lowers the depth of the doping potential by approximately 10%. However, this apparently mild effect on the doping potential leads to a significant lowering of the Fermi level (by approximately 50 meV).

If the short-range term (U_0) is ignored, our method can be applied to any 2D density, since Eq. (10) without U_0 is independent of the doping pattern. Table II shows the results (obtained with step 1 + XC) for Fermi level (relative to the conduction band minimum of bulk Si) for 2D doping density ranging from 6.6×10^{11} cm^{-2} to 1.7×10^{14} cm^{-2} (1/4 ML case). Note that including the U_0 term will push up the Fermi level by 12 meV for the maximal doping case and its effect on the lower doping cases should be much less. Our results indicate that the Fermi level goes progressively deeper as the doping concentration increases. The large range of variation
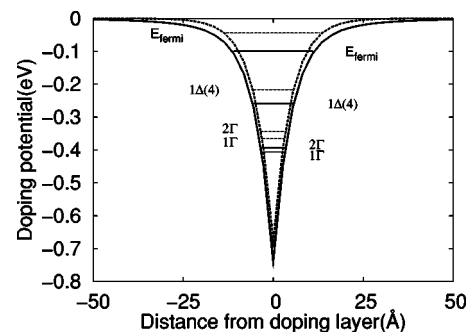

FIG. 3. Self-consistent potential profile of δ-doped Si. The lowest-lying confined states derived from each valley and the Fermi level are labeled. The right (left) labels are for results obtained with (without) the XC and SR effects.

TABLE II. Fermi level (E_F) (obtained with step 1+XC) versus doping density (n_{2D}).

ML	1/4	1/16	1/64	1/256	1/1024
$n_{2D}(10^{14}$ cm$^{-2})$	1.70	0.42	0.106	0.0265	0.0066
E_F (meV)	−111	−62	−36	−17	−8

of the Fermi level with respect to CBM offers a more flexible design for planar single-electron transistors (SETs), which can be constructed by using the δ-doped Si layer as conducting sheets separated by an undoped region (as barrier) and a nanoscale patch of δ-doped Si as the central island. This type of planar SETs can be more easily integrated with the quantum bits made of isolated phosphorous donors.

The distribution of carriers among different valleys as the density varies is also of interest. In Fig. 4, we show the fractional occupancy of carriers in the subbands derived from the z pockets (denoted as Γ valley) and the x,y pockets (denoted as Δ valley) as functions of the doping density in units of ML (monolayer). As shown in the figure, in the extremely low density limit, only the z pockets are populated. As the density increases, the population in the x,y pockets gains quickly and it exceeds the z-pocket population at $n_{2D} > 0.02$ ML (or 1.36×10^{13} cm^{-2}). For doping density between 0.1 and 0.25 ML, the carriers occupy the six pockets almost evenly. Since electrons in the z pockets have smaller in-plane effective mass, they can move faster than those electrons in the x,y pockets. Thus, our calculation indicates that the ratio in density of fast to slow electrons is large at the low-density limit and it quickly reduces as density increases and progressively approaches $1/2$ as n_{2D} approaches 0.25 ML.

IV. CONCLUSION

We have studied the self-consistent potential profile for phosphorus doping sheet embedded in Si (with concentration as high as a 1/4 monolayer), taking into account the full band structure effect with an empirical pseudopotential model. We find that for the highest doping (1/4 ML case), the Fermi level lies approximately 100 meV below the conduction-band minimum (CBM). With this model, we can examine the effect of the short-range part of the doping potential on the subband structure and Fermi level. The main
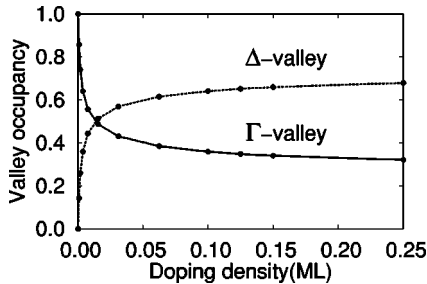

FIG. 4. Fractional occupancy among different valleys versus the doping density.

effect of the short-range interaction is to cause a shift in subband energies in the amount ~ 10 meV and modify the effective masses of the subbands by about 1%. Furthermore, the 1/4 ML patterning leads to zone-folding effect that causes mixing of the x-y valleys with the z valley. All these effects combined lead to a change in the Fermi level by about 10 meV. We have also studied the dependence of the Fermi level in the delta-doping junction as a function of the doping concentration and find that the separation between the Fermi level and bulk CBM varies significantly as the doping density changes. Our results provide useful design parameters for the future fabrication of planar single-electron transistors (SETs) made of phosphorous-doped Si, which can be easily integrated with the quantum bits made of isolated phosphorous donors. Here we have described a detailed microscopic approach for dealing with δ-doped systems and applied it to phosphorous (n-type) δ-doped silicon. The same method can also be applied to p-type δ-doped systems as well as δ doping in other host systems.

APPENDIX

In this appendix, we provide details of the derivation for matrix elements discussed in the text. The Fourier transform of the products of two PWO's is given by

$$\langle W_{n\mathbf{k}_s}(l_z)|e^{-i\mathbf{q}\cdot\mathbf{r}}|W_{n'\mathbf{k}_{s'}}(l_z')\rangle$$

$$= \sum_{\substack{\alpha\nu\sigma \\ \alpha'\nu'\sigma'}} \sum_{\mathbf{G}_\parallel,\mathbf{G}_\parallel'} IC^w_{n\mathbf{k}_s}(\alpha,\nu,\sigma)C^w_{n'\mathbf{k}_{s'}}(\alpha',\nu',\sigma')I_p(\Delta\mathbf{G},\Delta l_z),$$

$$(A1)$$

where

$$I \equiv \frac{1}{N_{2D}\sigma_{\text{cell}}} \int dz f^{\sigma'l_z'}_{\alpha'\nu'}(z) f^{\sigma l_z}_{\alpha\nu}(z)e^{iq_z z} \int d^2\rho e^{i(\Delta\mathbf{G}-\mathbf{q}_\parallel)\rho}$$

$$= \left(\int dz f^{\sigma l_z}_{\alpha\nu}(z) f^{\sigma'l_z'}_{\alpha'\nu'}(z)e^{iq_z z} \right)(2\pi)^2 \delta_{\mathbf{q}_\parallel,\Delta\mathbf{G}} \qquad (A2)$$

in which

$$\Delta_\mathbf{G} \equiv \mathbf{G}_\parallel + \mathbf{G}_s - \mathbf{G}_\parallel' - \mathbf{G}_{s'}.$$

Substituting Eqs. (5), (A1), and (A2) into Eq. (10), we have

$$\langle W_{n\mathbf{k}_s}(l_z)|V_{\text{dop}}(\mathbf{r})|W_{n'\mathbf{k}_{s'}}(l_z')\rangle$$

$$= \sum_{\substack{\alpha\nu\sigma \\ \alpha'\nu'\sigma'}} \int dz f^{\sigma l_z}_{\alpha\nu}(z) f^{\sigma'l_z'}_{\alpha'\nu'}(z)\frac{1}{\sigma_{\text{cell}}}\sum_{\mathbf{G}_\parallel,\mathbf{G}_\parallel'} \int \frac{dq_z}{2\pi}V_d(\Delta_G^2 + q_z^2)$$

$$\times e^{iq_z z}I_p(\Delta\mathbf{G},\Delta l_z)C^w_{n\mathbf{k}_s}(\alpha,\nu,\sigma)C^w_{n'\mathbf{k}_{s'}}(\alpha',\nu',\sigma'), \qquad (A3)$$

where

$$V_d(\Delta_G^2 + q_z^2)e^{iq_z z} = 8\pi Q \left[\frac{1}{\varepsilon(0)(\Delta_G^2 + q_z^2)} + \frac{A}{\Delta_G^2 + q_z^2 + \gamma_1^2} \right.$$
$$\left. + \frac{1-A}{\Delta_G^2 + q_z^2 + \gamma_2^2} - \frac{1}{\varepsilon(0)} \frac{1}{\Delta_G^2 + q_z^2 + \gamma_3^2} \right].$$

Using the formula

we have

$$\int_{-\infty}^{\infty} \frac{e^{-ipx}dx}{a^2 + x^2} = \frac{\pi}{a} e^{-|ap|} \tag{A4}$$

$$\langle W_{n\mathbf{k}_s}(l_z)|V_{\text{dop}}|W_{n'\mathbf{k}_{s'}}(l_z')\rangle = \sum_{\mathbf{G}_\|,\mathbf{G}_\|'} C_{n\mathbf{k}_s}^w(\alpha,\nu,\sigma) C_{n'\mathbf{k}_{s'}}^w(\alpha',\nu',\sigma') \frac{-4\pi Q}{\sigma_{\text{cell}}} \sum_{\substack{\alpha\nu\sigma \\ \alpha'\nu'\sigma'}} \int dz f_{\alpha'\nu'}^{\sigma'l_z'}(z) f_{\alpha\nu}^{\sigma l_z}(z) I_p(\Delta\mathbf{G},\Delta l_z)$$

$$\times \left[\frac{1}{\varepsilon(0)} \frac{e^{-|\Delta_\mathbf{G} z|}}{|\Delta_\mathbf{G}|} + A \frac{e^{-|\sqrt{\gamma_1^2 + \Delta_\mathbf{G}^2} z|}}{\sqrt{\gamma_1^2 + \Delta_\mathbf{G}^2}} + (1-A) \frac{e^{-|\sqrt{\gamma_2^2 + \Delta_\mathbf{G}^2} z|}}{\sqrt{\gamma_2^2 + \Delta_\mathbf{G}^2}} - \frac{1}{\varepsilon(0)} \frac{e^{-|\sqrt{\gamma_3^2 + \Delta_\mathbf{G}^2} z|}}{\sqrt{\gamma_3^2 + \Delta_\mathbf{G}^2}} \right]. \tag{A5}$$

Note that the first term in the above equation is divergent as $\Delta_\mathbf{G} \to 0$. In this long wavelength limit, we have

$$\lim_{\Delta_\mathbf{G} \to 0} \int dz f_{\alpha'\nu'}^{\sigma'l_z'}(z) f_{\alpha\nu}^{\sigma l_z}(z) \frac{1}{|\Delta_\mathbf{G}|} e^{-|\Delta_\mathbf{G} z|} = \int dz f_{\alpha'\nu'}^{\sigma'l_z'}(z) f_{\alpha\nu}^{\sigma l_z}(z) \frac{1}{|\Delta_\mathbf{G}|} [1 - |\Delta_\mathbf{G} z| + O(|\Delta_\mathbf{G} z|^2)] \approx \int dz \cdot f_{\alpha'\nu'}^{\sigma'l_z'}(z) f_{\alpha\nu}^{\sigma l_z}(z)(-|z|) + C(\infty)$$

$$= \left(-|l_z| \frac{a}{2} \right) \int dz f_{\alpha'\nu'}^{\sigma'l_z'}(z) f_{\alpha\nu}^{\sigma l_z}(z) + C(\infty). \tag{A6}$$

The first term corresponds to the long-range Coulomb potential of a uniformly charged sheet. The second term corresponds to the self-interaction Coulomb energy of an infinite charged sheet. This part will be cancelled exactly by the same contribution from the negatively charged doping electrons (in the Hartree term). The charge neutrality of the system guarantees the exact cancellation of the $C(\infty)$ term.

The remainder (nondivergent terms) are denoted by

$$U_0(\mathbf{k}_\|, n, n', l_z, l_z', \mathbf{G}_s, \mathbf{G}_{s'}) = \sum_{\mathbf{G}_\|,\mathbf{G}_\|'} \sum_{\substack{\alpha\nu\sigma \\ \alpha'\nu'\sigma'}} \frac{4\pi Q}{\sigma_{\text{cell}}} \int dz f_{\alpha'\nu'}^{\sigma'l_z'}(z) f_{\alpha\nu}^{\sigma l_z}(z) I_p(\Delta\mathbf{G}, \Delta l_z) C_{n\mathbf{k}_s}^w(\alpha,\nu,\sigma) C_{n'\mathbf{k}_{s'}}^w(\alpha',\nu',\sigma')$$

$$\times \left[\frac{1}{\varepsilon(0)} \frac{e^{-|\Delta_\mathbf{G} z|}}{|\Delta_\mathbf{G}|} \Delta_{G \neq 0} + A \frac{e^{-|\sqrt{\gamma_1^2 + \Delta_\mathbf{G}^2} z|}}{\sqrt{\gamma_1^2 + \Delta_\mathbf{G}^2}} + (1-A) \frac{e^{-|\sqrt{\gamma_2^2 + \Delta_\mathbf{G}^2} z|}}{\sqrt{\gamma_2^2 + \Delta_\mathbf{G}^2}} - \frac{1}{\varepsilon(0)} \frac{e^{-|\sqrt{\gamma_3^2 + \Delta_\mathbf{G}^2} z|}}{\sqrt{\gamma_3^2 + \Delta_\mathbf{G}^2}} \right]. \tag{A7}$$

The integrals are performed numerically via the Gaussian quadrature technique.

To reduce the computation effort, the integral can be tabulated as a function of ΔG^2, and calculated with interpolation method. The accuracy of the method can be checked in various ways. We have verified the numerical accuracy of the above approximation by the dense mesh method and by MATHEMATICA.

To calculate the short-range contribution, we take it to be the difference in s-like unscreened atomic pseudopotential for P and Si, obtained from first principles. It has the form

$$V_{\text{loc}}(r) = -\frac{1}{r} \text{erf}\left(\frac{1}{\sqrt{2}r_{\text{loc}}} \right) + f(r), \tag{A8}$$

where r_{loc} is the local core radius and $f(r)$ is a short-ranged function in numerical form. Since $\text{erf}(x) = 1 - \text{erfc}(x)$, we have

$$V_{\text{loc}}(r) = -\frac{1}{r} + \text{erfc}\left(\frac{1}{\sqrt{2}r_{\text{loc}}} \right) + f(r). \tag{A9}$$

The last two terms contain the short-range contribution. The short-range part of the screened pseudopotential is given by

$$V_{\text{ps}}(r) = \frac{1}{\varepsilon} V_{\text{loc}}(r) + \frac{1}{\varepsilon_0 r}.$$

The Fourier transformation of form $V_{\text{ps}}(r)$ can be fitted with linear combinations of Gaussian functions of the form

$$\tilde{V}_{\text{ps}}(\mathbf{q}) = \sum_l c_l e^{-\alpha_l \mathbf{q}^2}.$$

[1] D. P. DiVincenzo, Science **270**, 255 (1995); A. Ekert and R. Jozsa, Rev. Mod. Phys. **68**, 733 (1996).

[2] Charles H. Bennett and David P. DiVincenzo, Nature (London) **404**, 247 (2000).

[3] M. A. Nielsen and I. L. Chuang, *Quantum Computation and Quantum Information* (Cambridge University Press, 2000), and references therein.

[4] R. Vrijen, E. Yablonovitch, K. L. Wang, H. W. Jiang, A. Balandin, V. Roychowdhury, T. Man, and D. DiVincenzo, Phys. Rev. A **62**, 012306 (2000).

[5] B. E. Kane, Nature (London) **393**, 133 (1998).

[6] T.-C. Shen, C. Wang, G. C. Abeln, J. R. Tucker, J. W. Lyding, Ph. Avouris, and R. E. Walkup, Science **268**, 1590 (1995).

[7] J. R. Tucker and T. C. Shen, IEE J. Solid-State Electron Devices **42**, 1061 (1998).

[8] Y. Wang, M. J. Bronikowski, and R. J. Hamers, J. Phys. Chem. **98**, 5966 (1994).

[9] T.-C. Shen, J.-Y. Ji, M. A. Zudov, R.-R. Du, J. Kline, and J. R. Tucker, Appl. Phys. Lett. **80**, 1580 (2002).

[10] S. R. Schofield, N. J. Curson, M. Y. Simmons, F. J. Ruess, T. Hallam, L. Oberbeck, and R. G. Clark, Phys. Rev. Lett. **91**, 136104 (2003).

[11] I. Eisele, Superlattices Microstruct. **6**, 123 (1989).

[12] H. M. Li, W. X. Ni, M. Willander, K. F. Berggren, B. E. Sernelius, and G. V. Hansson, Thin Solid Films **183**, 331 (1989).

[13] L. M. R. Scolfaro, D. Beliaev, R. Enderlein, and J. R. Leite, Phys. Rev. B **50**, 8699 (1994).

[14] Y. C. Chang and G. Li, Comput. Phys. Commun. **95**, 158 (1996).

[15] J. Bernholc and Sokrates T. Pantelides, Phys. Rev. B **15**, 4935 (1977).

[16] S. T. Pantelides and C. T. Sah, Phys. Rev. B **10**, 621 (1974).

[17] W. Kohn and L. J. Sham, Phys. Rev. **140**, A1133 (1965).

[18] D. M. Ceperley and B. J. Alder, Phys. Rev. Lett. **45**, 566 (1980).

[19] J. Perdew and A. Zunger, Phys. Rev. B **23**, 5048 (1981).

[20] W. F. Brinkman and T. M. Rice, Phys. Rev. B **7**, 1508 (1973).

[21] M. Altareli, W. Y. Hsu, and R. A. Sabatini, J. Phys. C **10**, L605 (1977).

[22] Y. C. Chang and H. Yao, Phys. Rev. B **54**, 11 517 (1996).

[23] H. J. Gossmann and E. F. Schubert, CRC Crit. Rev. Solid State Mater. Sci. **18**, 1 (1993).